NANO LETTERS

pubs.acs.org/NanoLett Letter

# Large Nonlinear Transverse Conductivity and Berry Curvature in $KTaO_3$ Based Two-Dimensional Electron Gas

Jinfeng Zhai, Mattia Trama, Hao Liu, Zhifei Zhu, Yinyan Zhu, Carmine Antonio Perroni, Roberta Citro,* Pan He,* and Jian Shen*

Cite This: *Nano Lett.* 2023, 23, 11892−11898 Read Online

ACCESS | Metrics & More | Article Recommendations | Supporting Information

**ABSTRACT:** Two-dimensional electron gas (2DEG) at oxide interfaces exhibits various exotic properties stemming from interfacial inversion and symmetry breaking. In this work, we report large nonlinear transverse conductivities in the $LaAlO_3$/$KTaO_3$ interface 2DEG under *zero* magnetic field. Skew scattering was identified as the dominant origin based on the cubic scaling of nonlinear transverse conductivity with linear longitudinal conductivity and 3-fold symmetry. Moreover, gate-tunable nonlinear transport with pronounced peak and dip was observed and reproduced by our theoretical calculation. These results indicate the presence of Berry curvature hotspots and thus a large Berry curvature triplet at the oxide interface. Our theoretical calculations confirm the existence of large Berry curvatures from the avoided crossing of multiple 5d-orbit bands, orders of magnitude larger than that in transition-metal dichalcogenides. Nonlinear transport offers a new pathway to probe the Berry curvature at oxide interfaces and facilitates new applications in oxide nonlinear electronics.

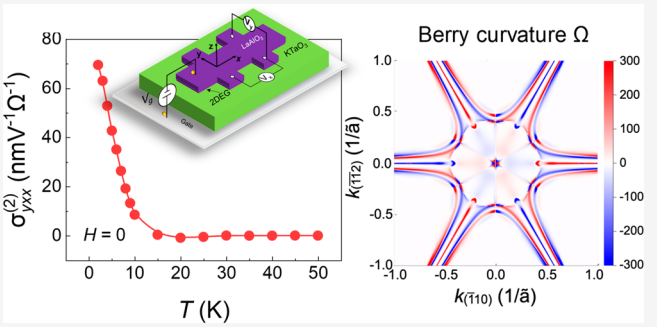


**KEYWORDS:** *oxide interface, two-dimensional electron gas, nonlinear Hall effect, gate tunability, Berry curvature triple*



Since the discovery of a highly mobile two-dimensional electron gas (2DEG) at the $LaAlO_3/SrTiO_3$ interface,[1] complex oxide heterostructures have attracted great interest. The oxide interface 2DEG exhibits exotic phenomena, including magnetism,[2] superconductivity,[3] and electric-field control of conductivity,[4] which are absent in their parent compounds. Due to the interfacial inversion symmetry breaking, Rashba spin−orbit coupling (SOC) leads to spin-polarized electronic bands, which facilitates efficient spin-charge interconversions[5,6] and novel spin dependent magneto-resistances.[7,8] These findings have sparked the field of oxide spintronics.[9] Recently, much of the attention has shifted to $KTaO_3$ (KTO) based 2DEG heterostructures, such as $LaTiO_3$/KTO,[10] $LaAlO_3$ (LAO)/KTO,[11] and EuO/KTO.[12] KTO is a band insulator, similar to $SrTiO_3$ with a high permittivity and quantum paraelectricity.[13] The atomic SOC, however, is much stronger in KTO (∼0.4 eV) than that in $SrTiO_3$. The KTO based 2DEG was found to show a higher critical temperature of superconductivity,[14−16] a larger spin-splitting of the Fermi surface,[17] and a more efficient spin-charge interconversion.[18,19] Due to the strong SOC, the absence of inversion symmetry at the interface, and multi-5d-orbits of KTO based 2DEGs, band anticrossings are expected to generate an enhanced Berry curvature, which encodes the geometric properties of the electronic wave functions. However, demonstrating its existence and effect on electron transport has not been explored.[20,21]

The linear Hall effect is forbidden under time-reversal symmetry.[22,23] However, the second-order nonlinear Hall effect (NHE) does not obey this constraint but requires inversion symmetry breaking. Following a predication by Sodemann and Fu,[24] NHE was recently observed in non-centrosymmetric $WTe_2$ under time-reversal symmetric conditions[25,26] from the Berry curvature dipole (BCD).[24] The transverse nonlinear transport can also arise also from the impurity scatterings, such as skew scattering[27,28] and side jump.[29] While the BCD driven NHE was found in crystals with one mirror reflection at maximum,[25,30] the skew scattering originated transverse nonlinear transport was recently observed in materials with three mirror reflections.[27,31] Skew scattering is due to the inherent chirality of itinerant electrons and exhibits a close relation to the Berry curvature.[27,28,31] It is allowed in all non-centrosymmetric time-reversal invariant materials. So far, transverse nonlinear transport has been

**Received:** October 14, 2023
**Revised:** December 7, 2023
**Accepted:** December 7, 2023
**Published:** December 11, 2023

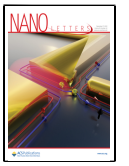





https://doi.org/10.1021/acs.nanolett.3c03948
*Nano Lett.* 2023, 23, 11892−11898

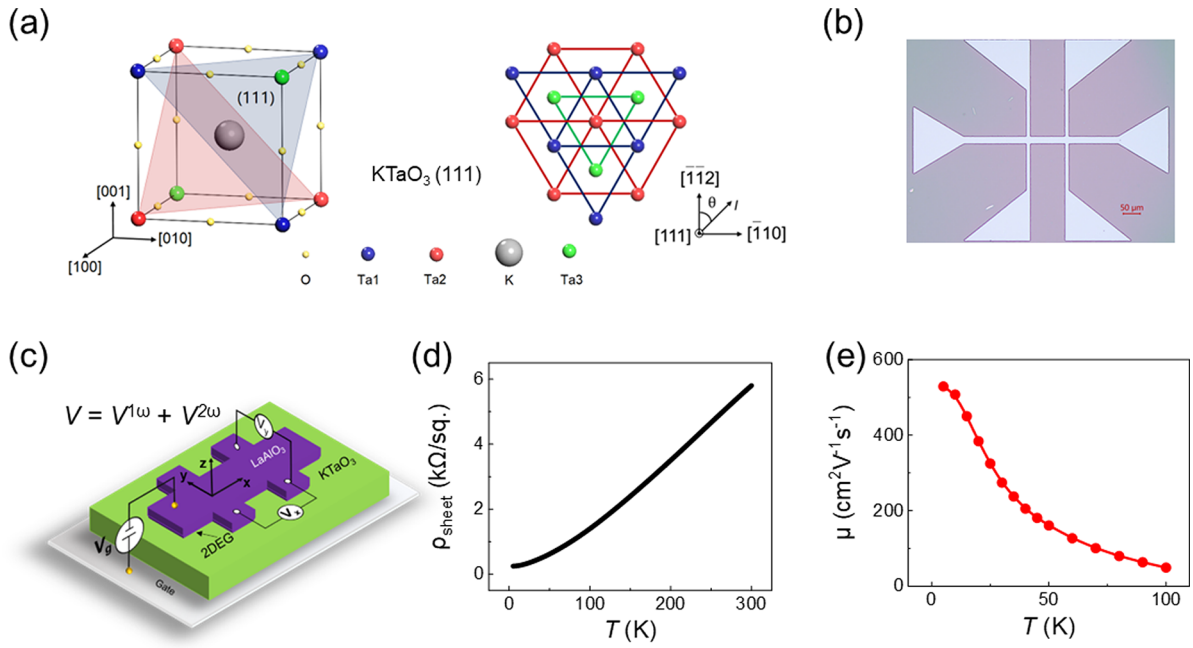


**Figure 1.** 2DEG at the $LaAlO_3/KTaO_3(111)$ interface and its basic transport characterizations. (a) Schematic unit cell of the perovskite $KTaO_3$ with the (111) plane shaded (left panel). Top view of three consecutive Ta layers on the (111) surface (right panel). The $[\bar{1}10]$ and $[\bar{1}\bar{1}2]$ axes are indicated. The current orientation angle $\theta$ with respect to the $[\bar{1}\bar{1}2]$ axis is indicated. (b) Optical image of a Hall bar. (c) Schematic of a field-effect device of LAO/KTO 2DEG and the electric harmonic measurements. A sinusoidal current $I^{\omega}$ was applied, and the first harmonic $V^{1\omega}$ and second harmonic $V^{2\omega}$ voltages were simultaneously measured at zero magnetic field along the longitudinal ($x$) and transverse ($y$) directions. The longitudinal voltage ($V_x$), transverse voltage ($V_y$), and gate voltage ($V_g$) are indicated. (d, e) The sheet resistance $\rho_{sheet}$ (d) and mobility $\mu$ (e) as a function of temperature.

widely studied in nonoxide materials.[29] Although oxide heterostructures represent a large family of materials with inversion symmetry breaking, a demonstration of transverse nonlinear transport is still lacking in these materials. The mechanisms for generating Berry curvature include SOC, orbit hybridization, etc.[32] It is thus highly desirable to study the Berry curvature related transverse nonlinear transport in KTO based 2DEG, which exhibits a large SOC and multiple d-orbit hybridizations.

In this paper, we report the observation of transverse nonlinear transport in the 2DEG at the LAO/KTO(111) interface up to room temperature (RT) under *zero* magnetic field. The nonlinear conductivity was found to decrease dramatically with rising temperature. Its scaling law with the longitudinal conductivity and the 3-fold symmetry establish skew scattering as the dominant physical origin. Moreover, a large and highly tunable nonlinear conductivity with peak and dip structures was observed by changing back-gate voltages, indicating the existence of large Berry curvature triples with sign changes. Our theoretical calculations show that the interplay of quantum confinement, strong SOC, and multi-d-orbits results in the generation of Berry curvature hotspots at the anticrossing bands and distributions of Berry curvature with sign changes. Nonlinear transport provides a new way to study topologically nontrivial band structures at the correlated oxide interfaces that differs from standard magneto-transport measurements.[33] The emergence of nonlinear transport will inject new momentum into the study of oxide heterostructures.

The LAO/KTO interfacial 2DEGs were prepared by growing an LAO overlayer mainly on single-crystalline KTO(111) substrates using pulsed laser deposition (see Supporting Information M1). The lattice structure of the KTO(111) surface is schematically shown in Figure 1a. Previous studies have shown that oxygen vacancies near the LAO/KTO interface can effectively electron dope the interfacial KTO.[34] Hall bar devices (Figure 1b) were fabricated via photolithography for transport measurements. As shown in Figure 1c, the linear and nonlinear electric transports can be separated by measuring the first harmonic ($V_i^{1\omega}$) and the second harmonic voltages ($V_i^{2\omega}$) under an ac current $I_x = I \sin \omega t$ using the lock-in techniques (Supporting Information M1) with $i$ representing the current direction $x$ or the transverse direction $y$. The LAO/KTO interface exhibits metallic behavior, as the sheet resistance $\rho_{sheet}$ increases monotonically with rising temperature in Figure 1d. Correspondingly, the carrier mobility $\mu$ shows a dramatic decrease with rising temperature in Figure 1e. Superconductivity is absent in this sample due to room temperature deposition.

To explore the transverse nonlinear transport under time-reversal symmetry, we measured the second-harmonic transverse voltage $V_y^{2\omega}$ at zero magnetic field. Figure 2a displays a sizable $V_y^{2\omega}$ for the current applied along the $[\bar{1}10]$ direction with a quadratic current dependence, i.e., $V_y^{2\omega} \propto I^2$. In contrast, a much smaller $V_y^{2\omega}$ was observed for the current applied along the $[\bar{1}\bar{1}2]$ direction (Supporting Information S1a). For both current directions, $V_y^{2\omega}$ changes sign when reversing the current and the corresponding Hall probes simultaneously (schematically shown in the inset of Figure 2a). We further revealed that $V_y^{2\omega}$ is independent of the ac frequency used and has a small contribution from the contact misalignment of the Hall device (Supporting Information S2), which may lead to a difference in magnitude of $V_y^{2\omega}$ under opposite currents. The dc biased ac measurements were also performed to further verify the observation of nonlinear transport (Supporting Information


https://doi.org/10.1021/acs.nanolett.3c03948
Nano Lett. 2023, 23, 11892−11898

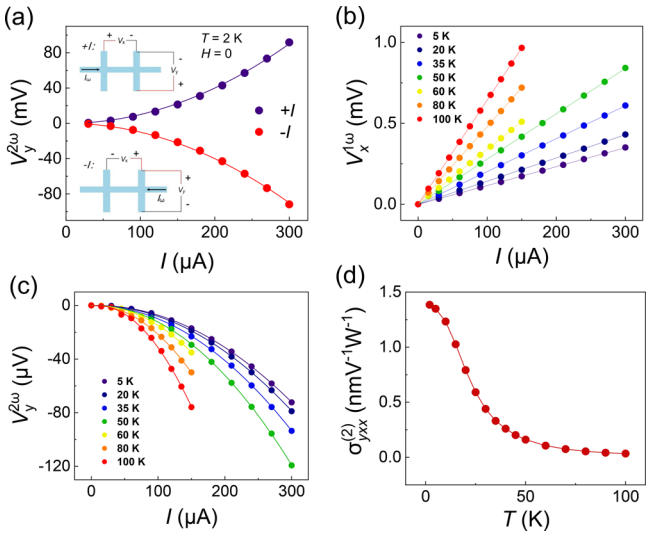


**Figure 2.** Observation of transverse nonlinear transport and its temperature dependence in LAO/KTO(111) 2DEG. (a) The second-harmonic transverse voltage $V_y^{2\omega}$ versus ac amplitude $I$ for the current along the $[\bar{1}10]$ axis. The solid curves are quadratic fits to the data. The insets show schematics of current and voltage probe connections under opposite currents of $+I$ and $-I$. The arrow indicates the current direction during the first half period of sinusoidal current. The data were collected at $T = 2$ K. (b) The first-harmonic longitudinal voltage $V_x^{1\omega}$ as a function of $I$ at different temperatures. The solid lines are linear fits to the data. (c) $V_y^{2\omega}$ versus $I$ at different temperatures. The solid curves are quadratic fits. (d) The nonlinear transverse conductivity $\sigma_{yxx}^{(2)}$ as a function of temperature. The data in parts a–d were measured under zero magnetic field in Sample 1.

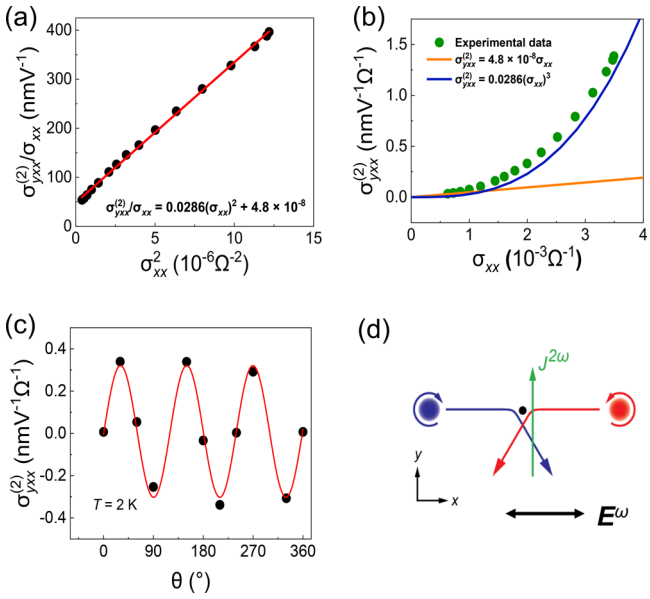


**Figure 3.** Scaling law of nonlinear transverse conductivity and its 3-fold symmetry. (a) The $\sigma_{yxx}^{(2)}/\sigma_{xx}$ versus $(\sigma_{xx})^2$. The red line is a linear fit to the experimental data. (b) The separated contributions to $\sigma_{yxx}^{(2)}$ as a function of $\sigma_{xx}$. The linear line (orange) represents the side jump contribution, while the cubic curve (blue) shows the skew scattering contribution. (c) The nonlinear transverse conductivity $\sigma_{yxx}^{(2)}$ versus the direction $\theta$ of current with respect to the $[\bar{1}\bar{1}2]$ axis. The red line is a sin $3\theta$ fit to the experimental data. (d) Schematic plot of the skew scattering at the LAO/KTO(111) interface and the induced nonlinear transverse transport. The blue and red balls represent self-rotating electron wave packets with opposite chirality (Berry curvature).

S2). These results unambiguously demonstrate the existence of transverse nonlinear transport at the LAO/KTO(111) interface under time-reversal symmetry.

To investigate the temperature dependence of transverse nonlinear transport, the $V_x^{1\omega}(I)$ and $V_y^{2\omega}(I)$ curves were measured simultaneously at different temperatures in Figure 2b and c, respectively. The linear dependence of $V_x^{1\omega}$ on $I$ indicates good ohmic contacts. The quadratic dependence of $V_y^{2\omega}$ on $I$ was observed at all of the temperatures. The nonlinear transverse conductivity $\sigma_{yxx}^{(2)}$ can then be calculated using the formula $\sigma_{yxx}^{(2)} = -\frac{\sigma_{xx}V_y^{2\omega}L^2}{(V_x^{1\omega})^2 W}$, where $\sigma_{xx}$ is the linear longitudinal conductivity and $L$ ($W$) is the length (width) of the Hall bar device.[31] A dramatic decrease of $\sigma_{yxx}^{(2)}$ with rising temperature was found in Figure 2d. To understand such temperature dependence, $\sigma_{yxx}^{(2)}/\sigma_{xx}$ is plotted as a function of $(\sigma_{xx})^2$ in Figure 3a. A good linear fit is shown as the red line. This scaling analysis can separate different contributions to the transverse nonlinear transport. Specifically, the linear slope corresponds to a $(\sigma_{xx})^3$ contribution to $\sigma_{yxx}^{(2)}$, which represents the skew scattering driven transverse nonlinear transport.[26,27] The nonzero intercept of the fitting corresponds to a $\sigma_{xx}$ linear contribution to $\sigma_{yxx}^{(2)}$, which originates from BCD or side jump.[24,26] Since KTO remains in the cubic phase down to 4.2 K,[35] the persistence of a 3-fold rotational symmetry for the (111) surface excludes the existence of BCD in the LAO/KTO(111) 2DEG.[17,24] Thus, the $\sigma_{xx}$ linear term is likely from the side jump, rather than BCD. This is different from $SrTiO_3$ based 2DEG that shows a cubic-to-tetragonal structural transition at 110 K, thus breaking the 3-fold rotational symmetry along the [111] direction and enabling a finite BCD.[36] Moreover, a 3-fold angular dependence of transverse nonlinear transport was observed in Figure 3c. It further supports the skew scattering origin and excludes the BCD origin, as the two mechanisms give rise to totally different angular dependences.[26,27] From the obtained fitting parameters, different contributions to $\sigma_{yxx}^{(2)}$ can be plotted as a function of $\sigma_{xx}$ in Figure 3b. We found transverse nonlinear transport arises dominantly from skew scattering in the highly conductive regime.[28,31] The wave packet of the Bloch electron self-rotates with a finite Berry curvature, and its chirality reverses with a change in the sign of the Berry curvature as schematically shown in Figure 3d.[27] Skew scattering arises from the chiral Bloch electron wave, whereby disorder deflects its motion in the preferred direction. It leads to the transverse nonlinear transport in non-centrosymmetric materials, as demonstrated previously in a gapped graphene and $Bi_2Se_3$ with Dirac cones.[27,28,31] Thus, the skew scattering related nonlinear transport acts as a hallmark of Berry curvature in the KTO based 2DEGs. Skew scattering can also give rise to longitudinal nonlinear transport with time-reversal symmetry as revealed in theory[28] and observed in experiment previously.[31]

It is worth noting that a sizable $V_y^{2\omega}$ was observed even at room temperature (RT) under a moderate current (Supporting Information S1b). This was achieved with the help of a high sheet resistance at RT (6 kΩ per square).[37] The voltage responsivity $\mathcal{R}_V$, defined as the ratio of the generated DC voltage to the power dissipation, is a figure of merit to quantify the conversion efficiency of rectifiers. $\mathcal{R}_V$ can be estimated as $\mathcal{R}_V = \frac{V_y^{2\omega}L}{\sigma_{xx}(V_x^{1\omega})^2 W} = 0.2V/W$ at RT and decreases with lowering


https://doi.org/10.1021/acs.nanolett.3c03948
Nano Lett. 2023, 23, 11892−11898

temperature, differing from $\sigma_{yxx}^{(2)}$ (Supporting Information S3). To enhance $\mathcal{R}_V$ for future applications, the interface engineering has to be optimized and a large $\sigma_{yxx}^{(2)}$ and a small $\sigma_{xx}$ are highly desirable. We highlight that the scalable sample preparation at RT makes KTO based 2DEGs promising materials for nonlinear device applications.

KTO has an extremely high dielectric constant (~5000 at 2 K), making it an ideal oxide for field effect application.[38] To study the field effect on nonlinear transport, back-gate voltages $V_g$ were applied between the bottom of the KTO substrate and the interfacial 2DEG (Figure 1c). Remarkably, while the longitudinal sheet resistance shows a monotonic decrease by 2 times with increasing $V_g$ from −40 V to +40 V in Figure 4a,[11,39] the nonlinear transverse resistance $R_{yx}^{2\omega} = V_y^{2\omega}/I$ shows a

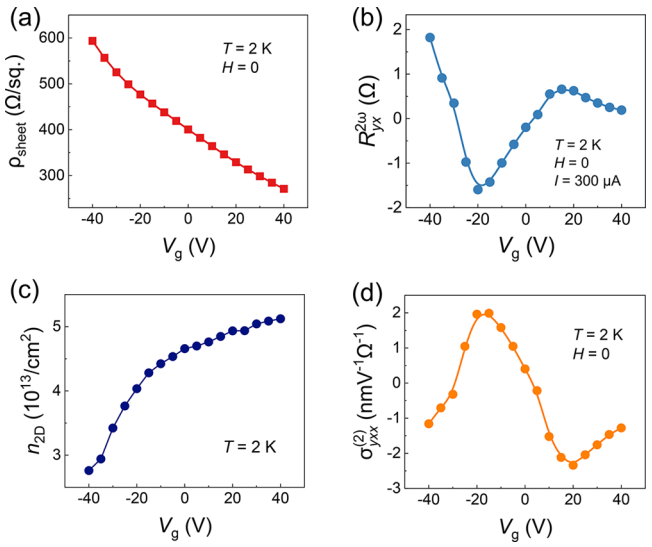


**Figure 4.** Back-gate dependence. (a) The sheet resistance $\rho_{sheet}$ versus gate voltage $V_g$. (b) The nonlinear transverse resistance $R_y^{2\omega}$ versus $V_g$. (c) The carrier density $n_{2D}$ versus $V_g$. (d) $\sigma_{yxx}^{(2)}$ versus $V_g$. The data in parts a−d were measured under zero magnetic field and at 2 K in Sample 1.

strong $V_g$ dependence with sign reversals, a peak and a dip in Figure 4b. The monotonic decrease of $\rho_{sheet}$ with $V_g$ can be mainly due to the fact that more electrons are occupying the bands, as estimated from the linear Hall effect measurements while scanning a magnetic field.[16] The variation of $V_g$ induces a $n_{2D}$ change of ~2.3 × $10^{13}$ $cm^{-2}$ in Figure 4c, which corresponds to a sizable Fermi energy variation. As a Fermi energy sensitive property, $\sigma_{yxx}^{(2)}$ is plotted as a function of $V_g$ in Figure 4d with a non-monotonic variation. Similar gate dependent results were obtained in other samples (Supporting Information S4). We note that such a large gate tunability of nonlinear transport has only been demonstrated before in 2D van der Waals materials.[25,31] $\sigma_{yxx}^{(2)}$ obtained in LAO/KTO(111) can be several times larger than that in $WTe_2$.[25,26]

To gain more insight into the gate dependence, the electronic band structure of 2DEG on the KTO(111) surface has been obtained in Figure 5a−c by performing a tight-binding supercell calculation (Supporting Information M2), which reproduces the angle-resolved photoemission spectroscopy results.[17] The 2DEG inherits the distinct properties of its parent bulk KTO, in addition to the quantum confinement effect at the surface. Specifically, the 2DEG is formed by the bands derived from the bulk $J$ = 3/2 doublet, which further generates the high-order sub-bands under the spatial confinement along the KTO[111] direction.[17] Tight-binding calculations suggested a strong mixing of $d_{xy}$, $d_{xz}$, and $d_{yz}$ orbitals driven by SOC[17,40,41] and a 6-fold symmetric Fermi surface consisting of star-shaped contours and hexagonal contours in Figure 5c. Note the band structures for 2DEG residing on the KTO(111) surface are different from that on the well-studied (001) surface.[11,39]

While the Rashba SOC has been widely studied at oxide interfaces,[39] the Berry curvature generation has rarely been explored. In this work, we calculated the Berry curvature distribution $\Omega_z(\mathbf{k})$ for the 2DEG on the KTO(111) surface (Supporting Information M2). The results for the two representative bands are shown in Figure 5d,e. The Berry curvature displays a significant momentum dependence and approaches maximum values (hotspots) at the $\mathbf{k}$ points in the vicinity of avoided band crossings, as the closer in energy the bands are, the more they contribute to the Berry curvature. The avoided crossing along the Γ−K direction extends over the full bandwidth of the system with a large Berry curvature as shown in Figure 5d, whereas the Berry curvature vanishes along Γ−M. The Berry curvature hotspots were also found close to the Γ−M direction when the different sub-bands intersect each other in Figure 5e. The distribution of Berry curvature is in line with the 3-fold symmetry of the KTO(111) surface, which enables a Berry curvature triple. It explains the 3-fold angular dependence of nonlinear transport observed in Figure 3c, showing a maximum value along $[\bar{1}10]$ and a small one along $[\bar{1}\bar{1}2]$ (see also Supporting Information S1). The typical Berry curvature near the anticrossing band structures is around 2000 Å$^2$, which is about 2 orders of magnitude larger than that in the well-studied transition-metal dichalcogenides (TMDC) at the $K$ points, such as $MoS_2$[42] ($\Omega_z \sim 9.88$ Å$^2$) and $WSe_2$[43] ($\Omega_z \sim 3.0$ Å$^2$). Another interesting observation is the presence of critical Fermi levels where the Berry curvature changes sign from a positive hotspot to a negative one. The nonlinear transverse conductivity has been calculated in Figure 5f based on the Berry curvature distribution and skew scattering theory, whereby $\sigma_{yxx}^{(2)} \propto \frac{e^3\tau^3}{p_F\tilde{\tau}}$ ($\tau$ is the symmetric scattering time, $\tilde{\tau}$ is the skew scattering time, $e$ is the electric charge, and $p_F$ is the Fermi momentum).[27,28] The calculation results are in line with our observation of gate dependent nonlinear transport with the peak and dip structures and sign changes in-between, re-establishing the explanation by skew scattering. The skew scattering driven nonlinear transport is enhanced at the Fermi energy with Berry curvature hotspots,[27,31] as the skew scattering rate $\tilde{\tau}^{-1}$ is proportional to the Berry curvature triple $T(\epsilon_F) = 2\pi\hbar \int \frac{d^2k}{(2\pi)^2}\delta(\epsilon_F - \epsilon_{\boldsymbol{k}})\Omega_z(\boldsymbol{k}) \cos 3\theta_k$ in the 3-fold system.[27] $T(\epsilon_F)$ quantifies the strength of the Berry curvature distribution on the Fermi surface of KTO(111) 2DEG, proposed in a topological insulator with a Dirac cone previously.[27] Transverse nonlinear transport shows peaks at the band filling to the anticrossing of band structure. In this sense, we can map gate dependent nonlinear transport to the topological band structure of the oxide 2DEG.[5] To establish the correspondence, the theoretical carrier density versus Fermi level has been calculated in Supporting Information S5. A small discrepancy between the theoretical carrier density and the experimental one was observed to achieve the nonlinear


https://doi.org/10.1021/acs.nanolett.3c03948
Nano Lett. 2023, 23, 11892−11898

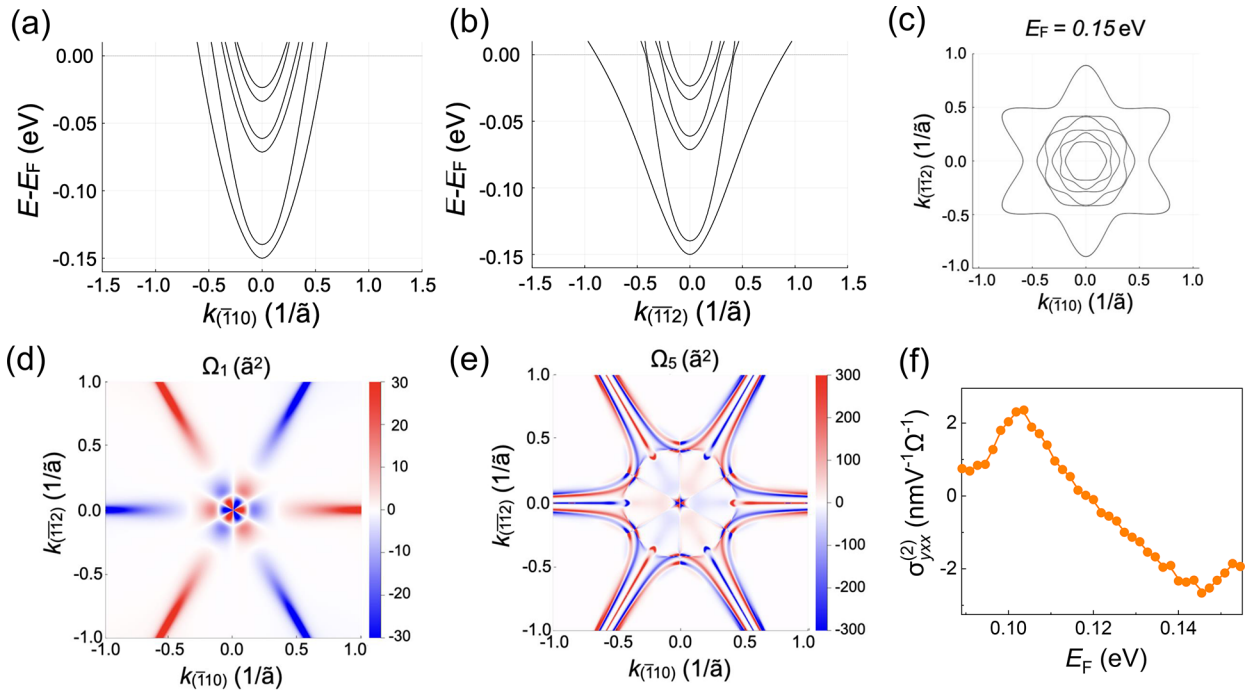


**Figure 5.** Calculated band structure and Berry curvature distribution for the 2DEG at the KTO(111) surface. (a, b) Tight-binding supercell calculation of electronic band structures along the $k[\bar{1}10]$ (Γ−K) (a) and $k[\bar{1}12]$ (Γ−M) (b) directions for the 2DEG on the KTO(111) surface. (c) Fermi surface for the benchmark choice of the Fermi level $E_F$ = 0.15 eV. (d−f) Berry curvature distribution in the $k$ space for one of the first (d) and third (e) doublets of the electronic band structure. The color bar indicates the magnitude of Berry curvature with $\tilde{a} = 0.3988 \times \sqrt{2/3}$ nm. (f) Theoretical nonlinear transverse conductivity $\sigma^{(2)}_{yxx}$ calculated based on the Berry curvature triple $T$ using the skew scattering theory with the coefficients chosen to best fit the experimental results.

conductivity peak. It can be due to the simplified model for the theoretical calculation, as reported in other studies.[39]

The transverse nonlinear transport was further observed in samples with different carrier densities, and it shows a similar temperature dependence (Supporting Information S6). The higher mobility sample shows a larger $\sigma^{(2)}_{yxx}$, consistent with the skew scattering theory. In addition, we deposited other overlayer material on the KTO(111) surface to induce the interface 2DEG, such as $Al_2O_3$. Similar nonlinear transport results have been obtained (Supporting Information S7). We may conclude that the nonlinear transport is a universal property for the KTO(111) based 2DEGs, irrespective of the carrier density or overlayer materials used. Moreover, we demonstrated the nonlinear transport in $SrTiO_3$ based 2DEGs with a similar temperature dependence and scaling behavior with the longitudinal conductivity (Supporting Information S8). Noting conducting oxide interfaces include a large pool of materials,[44] nonlinear transports are anticipated to exist in other oxide interfaces. Nonlinear transport can be further enhanced by interface-engineering of the artificial 2DEGs, such as the surface orientation of KTO, which can produce higher mobility samples.[45,46] The largest $\sigma^{(2)}_{yxx}$ of $7 \times 10^{-2}$ $\mu$m $\Omega^{-1}$ $V^{-1}$ was obtained at 2 K from a $KTaO_3$(001) 2DEG with a carrier mobility around 7500 $cm^2$ $V^{-1}$ $S^{-1}$ (Supporting Information S9). The nonlinear conductivity in $KTaO_3$ based 2DEG is larger than that of most reported materials such as $WTe_2$ but smaller than that in graphene (see Supporting Information Table S1 for a direct comparison). The nonlinear transport can also be applicable to the $KTaO_3$ based superconducting samples, providing an alternative method to study interfacial superconductors. It can also be further modulated by applying a magnetic field.[47] On the other hand, the large Berry curvature in the KTO based 2DEGs is expected to induce a large intrinsic spin Hall effect, which waits for future investigations.

In conclusion, we demonstrated the emergence of transverse nonlinear transport in the LAO/KTO interface 2DEG at zero magnetic field, which is sustained up to RT. A large nonlinear conductivity was found, which can be 2 orders of magnitude larger than that reported in $WTe_2$. With the absence of BCD and the existence of a Berry curvature triple, skew scattering dominates the nonlinear transport in the LAO/KTO(111) 2DEG. The skew scattering originating nonlinear transport was observed in an oxide system for the first time. The large SOC, quantum confinement, and multiorbital character have been utilized in this work to generate topological nontrivial bands with Berry curvature hotspots. The highly Fermi energy dependent Berry curvature distribution enables the nonlinear transport of the Bloch electron with a large gate tunability. Our results will stimulate the search for topological nontrivial band structures in other oxide heterostructures from the perspective of nonlinear transport. The nonlinear transport reported in this work provides a new method to explore the $KTO_3$ based interfacial superconductivity, which is currently of great interest.

## ■ ASSOCIATED CONTENT

### Data Availability Statement

All data needed to evaluate the conclusions in the paper are present in the paper and/or the Supporting Information.

### Supporting Information

The Supporting Information is available free of charge at https://pubs.acs.org/doi/10.1021/acs.nanolett.3c03948.



https://doi.org/10.1021/acs.nanolett.3c03948
Nano Lett. 2023, 23, 11892−11898

Sample preparation, transport measurements, nonlinear transport results along different crystal directions and at room temperature, analysis of contact misalignment and dc biased ac measurements, temperature dependences of voltage responsibility, gate dependent results for the LAO/KTO(111) Sample 2, theoretical model, calculations of carrier density, nonlinear transport for samples with different carrier densities, nonlinear transport at the $Al_2O_3$/KTO(111) interface, $SrTiO_3$(111) surface, and LAO/KTO(001) interface (PDF)

## AUTHOR INFORMATION


### Corresponding Authors

**Roberta Citro** − *Physics Department "E.R. Caianiello" and CNR-SPIN Salerno Unit, Universitá Degli Studi di Salerno, I-84084 Fisciano, Sa, Italy; INFN—Gruppo Collegato di Salerno, I-84084 Fisciano, Italy*; Email: rocitro@unisa.it

**Pan He** − *State Key Laboratory of Surface Physics and Institute for Nanoelectronic Devices and Quantum Computing, Fudan University, Shanghai 200433, China; Zhangjiang Fudan International Innovation Center, Fudan University, Shanghai 201210, China*; orcid.org/0000-0003-1462-7202; Email: hepan@fudan.edu.cn

**Jian Shen** − *State Key Laboratory of Surface Physics and Institute for Nanoelectronic Devices and Quantum Computing, Fudan University, Shanghai 200433, China; Zhangjiang Fudan International Innovation Center, Fudan University, Shanghai 201210, China; Department of Physics, Fudan University, Shanghai 200433, China; Shanghai Research Center for Quantum Sciences, Shanghai 201315, China; Collaborative Innovation Center of Advanced Microstructures, Nanjing 210093, China*; orcid.org/0000-0001-5670-1429; Email: shenj5494@fudan.edu.cn

### Authors

**Jinfeng Zhai** − *State Key Laboratory of Surface Physics and Institute for Nanoelectronic Devices and Quantum Computing, Fudan University, Shanghai 200433, China*; orcid.org/0000-0002-4017-6022

**Mattia Trama** − *Physics Department "E.R. Caianiello" and CNR-SPIN Salerno Unit, Universitá Degli Studi di Salerno, I-84084 Fisciano, Sa, Italy; INFN—Gruppo Collegato di Salerno, I-84084 Fisciano, Italy; Institute for Theoretical Solid State Physics, IFW Dresden, 01069 Dresden, Germany*

**Hao Liu** − *State Key Laboratory of Surface Physics and Institute for Nanoelectronic Devices and Quantum Computing, Fudan University, Shanghai 200433, China*

**Zhifei Zhu** − *State Key Laboratory of Surface Physics and Institute for Nanoelectronic Devices and Quantum Computing, Fudan University, Shanghai 200433, China*

**Yinyan Zhu** − *State Key Laboratory of Surface Physics and Institute for Nanoelectronic Devices and Quantum Computing, Fudan University, Shanghai 200433, China*

**Carmine Antonio Perroni** − *Physics Department "Ettore Pancini", Universitá Degli Studi di Napoli "Federico II", Complesso Univ. Monte S. Angelo, I-80126 Napoli, Italy; CNR-SPIN Napoli Unit and INFN Napoli Unit, Complesso Univ. Monte S. Angelo, I-80126 Napoli, Italy*

Complete contact information is available at: https://pubs.acs.org/10.1021/acs.nanolett.3c03948


### Author Contributions

J.Z. and M.T. contributed equally to this work. P.H. and J.S. planned the study. J.Z. grew the films, fabricated the devices, and performed the transport measurements with the help from Z.Z., H.L., and Y.Z. M.T., C.A.P., and R.C. performed the theoretical studies. All authors discussed the results. P.H., J.Z., M.T., R.C., and J.S. wrote the manuscript.

### Notes

The authors declare no competing financial interest.

## ACKNOWLEDGMENTS

This work was supported by the National Key Research and Development Program of China (Grant Nos. 2020YFA0308800 and 2022YFA1403300), National Natural Science Foundation of China (Grant No. 12174063), Natural Science Foundation of Shanghai (Grant Nos. 21ZR1404300 and 23ZR1403600), and the start-up funding from Fudan University. C.A.P. and R.C acknowledge founding from the PRIN 2022 PNRR project P2022SB73K - Superconductivity in KTaO3 Oxide-2DEG NAnodevices for Topological quantum Applications (SONATA). Part of the sample fabrication was conducted at Fudan Nanofabrication Lab.

## REFERENCES


(1) Ohtomo, A.; Hwang, H. Y. A high-mobility electron gas at the $LaAlO_3/SrTiO_3$ heterointerface. *Nature* **2004**, *427* (6973), 423−426.

(2) Brinkman, A.; Huijben, M.; van Zalk, M.; Huijben, J.; Zeitler, U.; Maan, J. C.; van der Wiel, W. G.; Rijnders, G.; Blank, D. H. A.; Hilgenkamp, H. Magnetic effects at the interface between non-magnetic oxides. *Nat. Mater.* **2007**, *6* (7), 493−496.

(3) Reyren, N.; Thiel, S.; Caviglia, A. D.; Kourkoutis, L. F.; Hammerl, G.; Richter, C.; Schneider, C. W.; Kopp, T.; Rüetschi, A.-S.; Jaccard, D.; et al. Superconducting Interfaces Between Insulating Oxides. *Science* **2007**, *317* (5842), 1196−1199.

(4) Caviglia, A. D.; Gariglio, S.; Reyren, N.; Jaccard, D.; Schneider, T.; Gabay, M.; Thiel, S.; Hammerl, G.; Mannhart, J.; Triscone, J. M. Electric field control of the $LaAlO_3/SrTiO_3$ interface ground state. *Nature* **2008**, *456* (7222), 624−627.

(5) Vaz, D. C.; Noël, P.; Johansson, A.; Göbel, B.; Bruno, F. Y.; Singh, G.; McKeown-Walker, S.; Trier, F.; Vicente-Arche, L. M.; Sander, A.; et al. Mapping spin-charge conversion to the band structure in a topological oxide two-dimensional electron gas. *Nat. Mater.* **2019**, *18* (11), 1187−1193.

(6) Lesne, E.; Fu, Y.; Oyarzun, S.; Rojas-Sánchez, J. C.; Vaz, D. C.; Naganuma, H.; Sicoli, G.; Attané, J. P.; Jamet, M.; Jacquet, E.; et al. Highly efficient and tunable spin-to-charge conversion through Rashba coupling at oxide interfaces. *Nat. Mater.* **2016**, *15* (12), 1261−1266.

(7) He, P.; Walker, S. M.; Zhang, S. S. L.; Bruno, F. Y.; Bahramy, M. S.; Lee, J. M.; Ramaswamy, R.; Cai, K.; Heinonen, O.; Vignale, G.; et al. Observation of Out-of-Plane Spin Texture in a $SrTiO_3$ (111) Two-Dimensional Electron Gas. *Phys. Rev. Lett.* **2018**, *120* (26), 266802.

(8) Choe, D.; Jin, M.-J.; Kim, S.-I.; Choi, H.-J.; Jo, J.; Oh, I.; Park, J.; Jin, H.; Koo, H. C.; Min, B.-C.; et al. Gate-tunable giant nonreciprocal charge transport in noncentrosymmetric oxide interfaces. *Nat. Commun.* **2019**, *10* (1), 4510.

(9) Trier, F.; Noël, P.; Kim, J.-V.; Attané, J.-P.; Vila, L.; Bibes, M. Oxide spin-orbitronics: spin-charge interconversion and topological spin textures. *Nat. Rev. Mater.* **2022**, *7* (4), 258−274.

(10) Zou, K.; Ismail-Beigi, S.; Kisslinger, K.; Shen, X.; Su, D.; Walker, F. J.; Ahn, C. H. $LaTiO_3/KTaO_3$ interfaces: A new two-dimensional electron gas system. *APL Materials* **2015**, *3* (3), 036104.

(11) Zhang, H.; Zhang, H.; Yan, X.; Zhang, X.; Zhang, Q.; Zhang, J.; Han, F.; Gu, L.; Liu, B.; Chen, Y.; et al. Highly Mobile Two-Dimensional Electron Gases with a Strong Gating Effect at the

Amorphous $LaAlO_3/KTaO_3$ Interface. *ACS Appl. Mater. Interfaces* **2017**, *9* (41), 36456−36461.
(12) Zhang, H.; Yun, Y.; Zhang, X.; Zhang, H.; Ma, Y.; Yan, X.; Wang, F.; Li, G.; Li, R.; Khan, T.; et al. High-Mobility Spin-Polarized Two-Dimensional Electron Gases at $EuO/KTaO_3$ Interfaces. *Phys. Rev. Lett.* **2018**, *121* (11), 116803.
(13) Samara, G. A.; Morosin, B. Anharmonic Effects in $KTaO_3$: Ferroelectric Mode, Thermal Expansion, and Compressibility. *Phys. Rev. B* **1973**, *8* (3), 1256−1264.
(14) Liu, C.; Yan, X.; Jin, D.; Ma, Y.; Hsiao, H.-W.; Lin, Y.; Bretz-Sullivan, T. M.; Zhou, X.; Pearson, J.; Fisher, B.; et al. Two-dimensional superconductivity and anisotropic transport at $KTaO_3$ (111) interfaces. *Science* **2021**, *371* (6530), 716−721.
(15) Chen, Z.; Liu, Z.; Sun, Y.; Chen, X.; Liu, Y.; Zhang, H.; Li, H.; Zhang, M.; Hong, S.; Ren, T.; et al. Two-Dimensional Superconductivity at the $LaAlO_3/KTaO_3$ (110) Heterointerface. *Phys. Rev. Lett.* **2021**, *126* (2), 026802.
(16) Chen, Z.; Liu, Y.; Zhang, H.; Liu, Z.; Tian, H.; Sun, Y.; Zhang, M.; Zhou, Y.; Sun, J.; Xie, Y. Electric field control of superconductivity at the $LaAlO_3/KTaO_3$ (111) interface. *Science* **2021**, *372* (6543), 721−724.
(17) Bruno, F. Y.; McKeown Walker, S.; Riccò, S.; de la Torre, A.; Wang, Z.; Tamai, A.; Kim, T. K.; Hoesch, M.; Bahramy, M. S.; Baumberger, F. Band Structure and Spin-Orbital Texture of the (111)-$KTaO_3$ 2D Electron Gas. *Adv. Electron. Mater.* **2019**, *5* (5), 1800860.
(18) Vicente-Arche, L. M.; Bréhin, J.; Varotto, S.; Cosset-Cheneau, M.; Mallik, S.; Salazar, R.; Noël, P.; Vaz, D. C.; Trier, F.; Bhattacharya, S.; et al. Spin-Charge Interconversion in $KTaO_3$ 2D Electron Gases. *Adv. Mater.* **2021**, *33* (43), 2102102.
(19) Zhang, H.; Ma, Y.; Zhang, H.; Chen, X.; Wang, S.; Li, G.; Yun, Y.; Yan, X.; Chen, Y.; Hu, F.; et al. Thermal Spin Injection and Inverse Edelstein Effect of the Two-Dimensional Electron Gas at $EuO$-$KTaO_3$ Interfaces. *Nano Lett.* **2019**, *19* (3), 1605−1612.
(20) Trama, M.; Cataudella, V.; Perroni, C. A.; Romeo, F.; Citro, R. Gate tunable anomalous Hall effect: Berry curvature probe at oxides interfaces. *Phys. Rev. B* **2022**, *106* (7), 075430.
(21) Wadehra, N.; Chakraverty, S. Emergent phenomena at interfaces of KTaO3. *Bulletin of Materials Science* **2021**, *44* (4), 269.
(22) Nagaosa, N.; Sinova, J.; Onoda, S.; MacDonald, A. H.; Ong, N. P. Anomalous Hall effect. *Rev. Mod. Phys.* **2010**, *82* (2), 1539−1592.
(23) Xiao, D.; Chang, M.-C.; Niu, Q. Berry phase effects on electronic properties. *Rev. Mod. Phys.* **2010**, *82* (3), 1959−2007.
(24) Sodemann, I.; Fu, L. Quantum Nonlinear Hall Effect Induced by Berry Curvature Dipole in Time-Reversal Invariant Materials. *Phys. Rev. Lett.* **2015**, *115* (21), 216806.
(25) Ma, Q.; Xu, S.-Y.; Shen, H.; MacNeill, D.; Fatemi, V.; Chang, T.-R.; Mier Valdivia, A. M.; Wu, S.; Du, Z.; Hsu, C.-H.; et al. Observation of the nonlinear Hall effect under time-reversal-symmetric conditions. *Nature* **2019**, *565* (7739), 337−342.
(26) Kang, K.; Li, T.; Sohn, E.; Shan, J.; Mak, K. F. Nonlinear anomalous Hall effect in few-layer WTe2. *Nat. Mater.* **2019**, *18* (4), 324−328.
(27) He, P.; Isobe, H.; Zhu, D.; Hsu, C.-H.; Fu, L.; Yang, H. Quantum frequency doubling in the topological insulator $Bi_2Se_3$. *Nat. Commun.* **2021**, *12* (1), 698.
(28) Isobe, H.; Xu, S.-Y.; Fu, L. High-frequency rectification via chiral Bloch electrons. *Sci. Adv.* **2020**, *6* (13), No. eaay2497.
(29) Du, Z. Z.; Lu, H.-Z.; Xie, X. C. Nonlinear Hall effects. *Nat. Rev. Phys.* **2021**, *3* (11), 744−752.
(30) Kumar, D.; Hsu, C.-H.; Sharma, R.; Chang, T.-R.; Yu, P.; Wang, J.; Eda, G.; Liang, G.; Yang, H. Room-temperature nonlinear Hall effect and wireless radiofrequency rectification in Weyl semimetal TaIrTe4. *Nat. Nanotechnol.* **2021**, *16* (4), 421−425.
(31) He, P.; Koon, G. K. W.; Isobe, H.; Tan, J. Y.; Hu, J.; Neto, A. H. C.; Fu, L.; Yang, H. Graphene moiré superlattices with giant quantum nonlinearity of chiral Bloch electrons. *Nat. Nanotechnol.* **2022**, *17* (4), 378−383.
(32) Gunnink, P. M.; Bouwmeester, R. L.; Brinkman, A. Artificial oxide heterostructures with non-trivial topology. *J. Phys.: Condens. Matter* **2020**, *33* (8), 085601.
(33) Kumar, N.; Wadehra, N.; Tomar, R.; Shama; Kumar, S.; Singh, Y.; Dattagupta, S.; Chakraverty, S. Observation of Shubnikov-de Haas Oscillations, Planar Hall Effect, and Anisotropic Magnetoresistance at the Conducting Interface of $EuO$-$KTaO_3$. *Adv. Quantum Technol.* **2021**, *4* (1), 2000081.
(34) Ojha, S. K.; Gogoi, S. K.; Mandal, P.; Kaushik, S. D.; Freeland, J. W.; Jain, M.; Middey, S. Oxygen vacancy induced electronic structure modification of $KTaO_3$. *Phys. Rev. B* **2021**, *103* (8), 085120.
(35) Wemple, S. H. Some Transport Properties of Oxygen-Deficient Single-Crystal Potassium Tantalate ($KTaO_3$). *Phys. Rev.* **1965**, *137* (5A), A1575−A1582.
(36) Lesne, E.; Sağlam, Y. G.; Battilomo, R.; Mercaldo, M. T.; van Thiel, T. C.; Filippozzi, U.; Noce, C.; Cuoco, M.; Steele, G. A.; Ortix, C.; et al. Designing spin and orbital sources of Berry curvature at oxide interfaces. *Nat. Mater.* **2023**, *22* (5), 576−582.
(37) Huang, M.; Wu, Z.; Hu, J.; Cai, X.; Li, E.; An, L.; Feng, X.; Ye, Z.; Lin, N.; Law, K. T.; et al. Giant nonlinear Hall effect in twisted bilayer WSe2. *National Science Review* **2023**, *10* (4), nwac232.
(38) Nakamura, H.; Kimura, T. Electric field tuning of spin-orbit coupling in $KTaO_3$ field-effect transistors. *Phys. Rev. B* **2009**, *80* (12), No. 121308.
(39) Zhang, H.; Yan, X.; Zhang, X.; Wang, S.; Xiong, C.; Zhang, H.; Qi, S.; Zhang, J.; Han, F.; Wu, N.; et al. Unusual Electric and Optical Tuning of KTaO3-Based Two-Dimensional Electron Gases with 5d Orbitals. *ACS Nano* **2019**, *13* (1), 609−615.
(40) Santander-Syro, A. F.; Bareille, C.; Fortuna, F.; Copie, O.; Gabay, M.; Bertran, F.; Taleb-Ibrahimi, A.; Le Fèvre, P.; Herranz, G.; Reyren, N.; et al. Orbital symmetry reconstruction and strong mass renormalization in the two-dimensional electron gas at the surface of $KTaO_3$. *Phys. Rev. B* **2012**, *86* (12), No. 121107.
(41) King, P. D. C.; He, R. H.; Eknapakul, T.; Buaphet, P.; Mo, S. K.; Kaneko, Y.; Harashima, S.; Hikita, Y.; Bahramy, M. S.; Bell, C.; et al. Subband Structure of a Two-Dimensional Electron Gas Formed at the Polar Surface of the Strong Spin-Orbit Perovskite $KTaO_3$. *Phys. Rev. Lett.* **2012**, *108* (11), 117602.
(42) Xiao, D.; Liu, G.-B.; Feng, W.; Xu, X.; Yao, W. Coupled Spin and Valley Physics in Monolayers of $MoS_2$ and Other Group-VI Dichalcogenides. *Phys. Rev. Lett.* **2012**, *108* (19), 196802.
(43) Cho, S.; Park, J.-H.; Hong, J.; Jung, J.; Kim, B. S.; Han, G.; Kyung, W.; Kim, Y.; Mo, S. K.; Denlinger, J. D.; et al. Experimental Observation of Hidden Berry Curvature in Inversion-Symmetric Bulk 2H-$WSe_2$. *Phys. Rev. Lett.* **2018**, *121* (18), 186401.
(44) Hwang, H. Y.; Iwasa, Y.; Kawasaki, M.; Keimer, B.; Nagaosa, N.; Tokura, Y. Emergent phenomena at oxide interfaces. *Nat. Mater.* **2012**, *11* (2), 103−113.
(45) Harashima, S.; Bell, C.; Kim, M.; Yajima, T.; Hikita, Y.; Hwang, H. Y. Coexistence of two-dimensional and three-dimensional Shubnikov-de Haas oscillations in $Ar^+$-irradiated $KTaO_3$. *Phys. Rev. B* **2013**, *88* (8), 085102.
(46) Zhang, H.; Yan, X.; Zhang, J.; Zhang, J.; Han, F.; Huang, H.; Qi, S.; Shi, W.; Shen, B.; Sun, J. The effect of fabrication conditions on 2DEGs transport characteristics at amorphous-$LaAlO_3/KTaO_3$ interfaces. *Mater. Res. Express.* **2019**, *6* (8), 086448.
(47) He, P.; Zhang, S. S. L.; Zhu, D.; Shi, S.; Heinonen, O. G.; Vignale, G.; Yang, H. Nonlinear Planar Hall Effect. *Phys. Rev. Lett.* **2019**, *123* (1), 016801.


https://doi.org/10.1021/acs.nanolett.3c03948
*Nano Lett.* 2023, 23, 11892−11898